Accelerating target-oriented multi-parameter elastic full-waveform uncertainty estimation by reciprocity

Mulder, W. A.; Kuvshinov, B. N.

Important note
To cite this publication, please use the final published version (if applicable).
Please check the document version above.

ORIGINAL ARTICLE

Accelerating target-oriented multi-parameter elastic full-waveform uncertainty estimation by reciprocity

W. A. Mulder[1,2] | **B. N. Kuvshinov[1]**

[1]Shell Global Solutions International B.V., Den Haag, The Netherlands

[2]Department of Geoscience & Engineering, Faculty of Civil Engineering and Geosciences, Delft University of Technology, Delft, The Netherlands

Correspondence

W. A. Mulder, Department of Geoscience & Engineering, Faculty of Civil Engineering and Geosciences, Delft University of Technology, Stevinweg 1, 2628 CN Delft, Delft, The Netherlands.
Email: w.a.mulder@tudelft.nl

Funding information

Shell Global Solutions International B.V.

Abstract

The accuracy of a model obtained by multi-parameter full-waveform inversion can be estimated by analysing the sensitivity of the data to perturbations of the model parameters in selected subsurface points. Each perturbation requires the computation of the seismic response in the form of Born scattering data for a typically very large number of shots, making the method time consuming. The computational cost can be significantly reduced by placing sources of different types at the Born scatterer, the point where the subsurface parameters are perturbed. Instead of modelling each shot separately, reciprocity relations provide the wavefields from the shot positions to the scatter point in terms of wavefields from the scatterer to the shot positions. In this way, the Born scattering data from a single point in the isotropic elastic case for a marine acquisition with pressure sources and receivers can be expressed in terms of the wavefields for force and moment tensor sources located at the scatterer and only a small number of forward runs are required. A two-dimensional example illustrates how the result can be used to determine the Hessian and local relative covariance matrix for the model parameters at the scatterer at the cost of five forward simulations. In three dimensions, that would be nine.

KEYWORDS

computing aspects, elastics, full waveform, parameter estimation, seismics

INTRODUCTION

Proper characterization of the underground conditions including uncertainty quantification is required in applications such as seismic exploration, monitoring of existing hydrocarbon reservoirs, storage of CO_2 or H_2 and using the subsurface for reliable geothermal energy. The subsurface is described by a set of model parameters that can be reconstructed by minimizing the misfit between the observed and the simulated data. The accuracy of the reconstruction depends on the sensitivity of the data to perturbations of the model parameters, commonly characterized by the second derivatives, or Hessian, of the misfit function at the global minimum. The pseudo-inverse of the Hessian is proportional to the covariance matrix of the model parameters in the maximum likelihood estimator (Backus & Gilbert, 1970; Tarantola, 2005).

In seismic subsurface characterization, the number of model parameters is very large, up to the order of a billion. This number squared is the size of the Hessian, making it computationally out of reach in terms of storage and compute time. For smaller 2-D problems, however, its direct computation is feasible on a dense grid (Pratt et al., 1998) or in isolated points (Hak & Mulder, 2010; Plessix & Mulder, 2004, for instance). Otherwise, approximations can be considered and there is a large body of literature on this topic including the Lanczos algorithm (Minkoff, 1996; Vasco et al., 2003), Kalman

filtering (Hoffmann et al., 2024; Thurin et al., 2017), low-rank approximations (Riffaud et al., 2024; Zhu et al., 2016) and Markov-chain Monte Carlo methods (Ely et al., 2018; Fichtner & van Leeuwen, 2015; Martin et al., 2012). The Hamiltonian Markov-chain Monte Carlo method (Betancourt, 2018; Duane et al., 1987) combines gradient-based minimization with uncertainty characterization and can be used for 2-D problems of modest size. Early applications to full-waveform inversion include a real-data example (Revelo Obando, 2018) and a synthetic one (Zhao & Sen, 2021). Fichtner and Zunino (2019) present a variant. Variational inference (Biswas et al., 2023; Izzatullah et al., 2023; Liu & Wang, 2016; Wang et al., 2023; Zhang & Curtis, 2020) allows for probability distributions other than Gaussian. Machine learning will also provide results (Rizzuti et al., 2020; Siahkoohi et al., 2023).

As already mentioned, instead of evaluating the full Hessian, a low-rank approximation is often used. A singular value decomposition, where only large eigenvalues of the Hessian are taken into account, is suited for preconditioning full-waveform inversion. Such an approach, however, is not beneficial for uncertainty evaluation, which is controlled by the small eigenvalues of the Hessian.

Alternatively, one can consider checkerboard perturbations (Inoue et al., 1990; Lévêque et al., 1993), perturbations of geological units (Mulder & Kuvshinov, 2023) and simultaneous perturbations on a sparse set of grid points (Chen & Xie, 2015; Rickett, 2003). The calculations might be still time consuming if one needs to model many shots.

While evaluating full-waveform inversion uncertainties everywhere in the subsurface might be of interest, interpretators find certain locations more important. Their focus is primarily on rock properties at certain points at the reservoir level, as these are key to understanding hydrocarbon accumulations and identifying faults. Such points are typically sparse, and their number is far smaller than the total number of grid points. The most valuable insights come from considering targeted perturbations of formation parameters at these specific points, where the information is most relevant, which requires only a subset of the full Hessian.

In this paper, we introduce a procedure to reduce the modelling time in cases where the number of shots is much larger than the number of perturbations under consideration. We treat the points where the model parameters are perturbed as Born scatterers. Instead of modelling actual shots, we simulate only a few shots with a number of different source types placed at the positions of the scatterers. The actual Born data are then reconstructed using reciprocity.

The reciprocity theorem is a common tool in seismic applications (De Hoop, 1966, 1988; Fokkema & van den Berg, 1993; Knopoff & Gangi, 1959). It states that a field at point *A* due to a source at point *B* is related to a field at point *B* due to a source at point *A*. Reciprocity can be of the convolution or correlation type (Bojarski, 1983; Wapenaar & Fokkema, 1993; Wapenaar, 1996). Arntsen and Carcione (2000) derived

reciprocity relations for inhomogeneous, anisotropic, viscoelastic solids involving different types of sources. Ikelle and Amundsen (2000) used reciprocity to model Born data in a water–solid configuration.

Our approach is similar to the latter, but we model water as an elastic solid with zero shear-wave velocity and adopt the second-order instead of a first-order form of the equations, leading to unified and simpler expressions. The required reciprocity expressions are derived in Appendix A for an arbitrary linear operator. When applied to the viscoelastic case, the results are nearly the same as those of Arntsen and Carcione (2000), correcting some sign problems and accounting for the symmetry of the strain and moment tensors. The method enables the construction of a local subset of the Hessian, describing the conditional uncertainty for the model parameters at the selected set of subsurface points.

To test and illustrate the capabilities of the method, we consider a 2-D marine example for the isotropic elastic case with an explosive source and pressure data. Cost estimates for a number of methods are included.

METHOD

Hessian and uncertainty

The least-squares misfit functional for observed data $\mathbf{d}^{\text{obs}}$, modelled by an operator $\mathcal{F}(\mathbf{m})$ with model parameters $\mathbf{m}$, has the form $\mathcal{X}(\mathbf{m}) = \frac{1}{2}\|\mathcal{F}(\mathbf{m}) - \mathbf{d}^{\text{obs}}\|^2$. It has a minimum at the model $\mathbf{m}_0$, hopefully, the global minimum. The uncertainty can be characterized by all models that obey

$$\mathcal{X}(\mathbf{m}_0 + \delta\mathbf{m}) \leq \varepsilon. \quad (1)$$

The threshold ε at the right-hand side is an estimate of the noise energy (Backus & Gilbert, 1970). In what follows, we sidestep the issue of how to determine a suitable value for ε and only consider uncertainty in a relative sense. The Taylor series expansion of the misfit functional around its minimum is

$$\mathcal{X} = \mathcal{X}_0 + \mathbf{g}^\top \delta\mathbf{m} + \frac{1}{2}\delta\mathbf{m}^\top \mathbf{H}\, \delta\mathbf{m} + \cdots, \quad (2)$$

with model perturbations $\delta\mathbf{m} = \mathbf{m} - \mathbf{m}_0$, gradient $\mathbf{g} = \nabla_{\mathbf{m}}\mathcal{X}(\mathbf{m}_0)$ and Hessian $\mathbf{H}$. In ideal situations, but not in practice, $\mathcal{X}_0 = 0$ and $\mathbf{g} = \mathbf{0}$.

For an assumed Gaussian distribution, variations of the model parameters $\delta\mathbf{m}$ are distributed as $p(\delta\mathbf{m}) \propto \exp\left[-\delta\mathbf{m}^\top \mathbf{H}\, \delta\mathbf{m}/(2\varepsilon)\right]$ (Tarantola, 2005). The pseudo-inverse of the Hessian (see Ben-Israel & Greville, 2003) is the covariance matrix $\mathbf{C} = \mathbf{H}^\dagger$. A conditional distribution is obtained by considering a subset of the model parameters, assuming the rest is known. The covariance matrix for the conditional distribution is determined by the
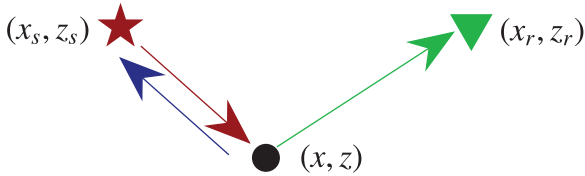
FIGURE 1 The incoming field from a source to a scatterer (red arrow) can be determined by reciprocity from fields propagating from the scatterer to the source (blue arrow). The Born scattering data can be synthesized by combining these fields with those from the scatterer to a receiver (green arrow).

pseudo-inverse of the associated subset of the Hessian **H**. Integrating over the model parameters outside the chosen subset results in a marginal distribution. The corresponding covariance matrix follows from the part of the full covariance matrix **C** that describes the subset.

The Hessian in the Gauss–Newton approximation equals $\mathbf{H} = \mathbf{F}^{\mathsf{T}}\mathbf{F}$, where $\mathbf{F} = \nabla_{\mathbf{m}}\mathcal{F}(\mathbf{m}_0)$ contains the Fréchet derivatives of the model operator. The Fréchet derivative $\nabla_{m_j}\mathcal{F}$ with respect to a single model parameter m_j can be found by perturbing m_j and determining the associated changes of the modelled data. Cross-correlating Fréchet derivatives, represented by Born scattering data, for each pair of model parameters, provides the full Hessian (Pratt et al., 1998). An alternative implementation is forward modelling followed by migration for perturbations of model parameters.

Calculation of the full Hessian is not feasible for large surveys. In this case, one can analyse uncertainty with respect to a small subset of the model. Even such an analysis is time consuming because, for each perturbation of a model parameter, one needs to simulate all the shots in the survey. The computational cost is significantly reduced by considering the perturbation as a Born scatterer and using reciprocity.

Figure 1 sketches the idea in two dimensions. A source at (x_s, z_s) generates the incoming field, indicated by the red arrow, which is scattered at (x, z) towards a receiver at (x_r, z_r), indicated by the green arrow. Reciprocity enables the replacement of a field propagating from source to scatterer (red arrow) by another field propagating from scatterer to source, indicated by the blue arrow.

In this way, one finds all the fields of a certain type incoming from the sources to the scatterer and scattered towards the receivers with one shot where a source is placed at the scatter point. In the constant-density acoustic case, this can be accomplished by a single shot. In the elastic case, several shots with different source characteristics are required. The fields propagating from the sources to the scatterer and from the scatterer to the receivers are combined to find $\nabla_{m_j}\mathcal{F}$ for a model perturbation m_j.

The equations required to implement the method for a viscoelastic medium are presented in the next section.

Calculation of scattered fields

We review the Born approximation of the system of elastic wave equations, mainly to introduce our notation and show where reciprocity is applied. The waves generated by a force $\mathbf{f}(\mathbf{x}, t)$ and propagating in the viscoelastic medium are described by the equation

$$\mathcal{L}\,\mathbf{u}(\mathbf{x}, t) = \mathbf{f}(\mathbf{x}, t). \tag{3}$$

Here, $\mathbf{u}$ is the displacement, t is time, $\mathbf{x}$ is the spatial coordinate and

$$(\mathcal{L}\mathbf{u})_i = \rho\partial_{tt}^2 u_i - \partial_{x_j}\left(\psi_{ijkl} \star \varepsilon_{kl}\right), \tag{4}$$

where ρ is the density, ψ_{ijkl} is the viscoelasticity tensor, ε_{kl} is the strain tensor, the star '$\star$' denotes convolution in the time domain and summation over repeated Latin indices is implied. The second equation (4) is obtained using the symmetry property $\psi_{ijkl} = \psi_{jikl}$. The operator $\mathcal{L}$ is self-adjoint in the sense that the condition $\langle\mathbf{u}', \mathcal{L}\mathbf{u}\rangle = \langle\mathcal{L}^\dagger\mathbf{u}', \mathbf{u}\rangle$, where the angular brackets are defined by Equation (A.2), is satisfied for $\mathcal{L}^\dagger = \mathcal{L}$. We consider three types of point forces (delta functions in space), with components

$$f_i^{(\alpha)}(\mathbf{x}, \mathbf{x}_s) = \delta_{i\alpha}\delta(\mathbf{x} - \mathbf{x}_s),$$
$$f_i^{(\alpha\beta)}(\mathbf{x}, \mathbf{x}_s) = \tfrac{1}{2}\left(\delta_{i\alpha}\partial_{x_\beta} + \delta_{i\beta}\partial_{x_\alpha}\right)\delta(\mathbf{x} - \mathbf{x}_s),$$
$$f_i^{(0)}(\mathbf{x}, \mathbf{x}_s) = \sum_\alpha f_i^{(\alpha\alpha)}(\mathbf{x}, \mathbf{x}_s) = \partial_{x_i}\delta(\mathbf{x} - \mathbf{x}_s). \tag{5}$$

The related solutions of Equation (3) are labelled as $\mathbf{u}^{(\alpha)}(\mathbf{x}, \mathbf{x}_s)$, $\mathbf{u}^{(\alpha\beta)}(\mathbf{x}, \mathbf{x}_s)$ and $\mathbf{u}^{(0)}(\mathbf{x}, \mathbf{x}_s)$. The associated volumetric strain $\varphi(\mathbf{x}, \mathbf{x}_s)$ and the strain tensor $\varepsilon_{ij}(\mathbf{x}, \mathbf{x}_s)$ are labelled accordingly, using the superscripts (α), $(\alpha\beta)$ or (0). We differentiate Equation (3) in the case of $f_i^{(\alpha)}$ with respect to the components α and β of $\mathbf{x}_s$. Taking into account that $\partial_{x_{s,\beta}}\delta(\mathbf{x} - \mathbf{x}_s) = -\partial_{x_\beta}\delta(\mathbf{x} - \mathbf{x}_s)$ and that $\mathcal{L}$ does not depend on $\mathbf{x}_s$ we conclude that

$$\tfrac{1}{2}\left(\partial_{x_{s,\beta}}\mathbf{u}^{(\alpha)} + \partial_{x_{s,\alpha}}\mathbf{u}^{(\beta)}\right) = -\mathbf{u}^{(\alpha\beta)}. \tag{6}$$

Similar relations hold for $\varphi^{(\alpha)}$ and $\varepsilon_{ij}^{(\alpha)}$.

In what follows, we analyse Equation (3) in the frequency domain, so that all the variables that depend on time are replaced by their frequency components. Let $\mathbf{u}$ be the solution of the equation

$$\mathcal{L}\mathbf{u} = \mathbf{f}, \tag{7}$$

for given force $\mathbf{f}$ and distribution of parameters $\rho(\mathbf{x})$ and $\psi_{ijkl}(\mathbf{x})$. If these parameters are perturbed by values $\delta\rho$ and $\delta\psi_{ijkl}$, the corresponding solution deviates from $\mathbf{u}$ by the value $\delta\mathbf{u}$. In the Born approximation, $\delta\mathbf{u}$ is governed by the

equation

$$(\mathcal{L}\delta\mathbf{u})_i = \omega^2 u_i \delta\rho + \partial_{x_j}\left(\varepsilon_{kl}\delta\psi_{ijkl}\right).$$ (8)

Here, we took into account that convolution in the time domain reduces to multiplication in the frequency domain. Since $\mathbf{u}^{(\alpha)}(\mathbf{x}, \mathbf{x}_s)$ is the Green function for Equation (3), the solution of Equation (8), is (Beylkin & Burridge, 1990; Hudson & Heritage, 1981; Kazei & Alkhalifah, 2019; Shaw & Sen, 2004; Snieder, 1986)

$$\delta\mathbf{u}(\mathbf{x}) = \int \mathbf{u}^{(i)}(\mathbf{x}, \mathbf{x}')\{\omega^2 u_i(\mathbf{x}')\delta\rho(\mathbf{x}')+$$
$$\partial_{x'_j}\left[\varepsilon_{kl}(\mathbf{x}')\delta\psi_{ijkl}(\mathbf{x}')\right]\} \, d\mathbf{x}'.$$ (9)

We integrate the second term in Equation (9) by parts. Taking into account that $\partial_{x'_j}\mathbf{u}^{(i)}\psi_{ijkl} = \frac{1}{2}(\partial_{x'_j}\mathbf{u}^{(i)} + \partial_{x'_i}\mathbf{u}^{(j)})\psi_{ijkl}$, due to the symmetry property of the viscoelasticity tensor $\psi_{ijkl} = \psi_{jikl}$, and using Equation (6), we obtain

$$\delta\mathbf{u}(\mathbf{x}) = \omega^2 \int \mathbf{u}^{(i)}(\mathbf{x}, \mathbf{x}')u_i(\mathbf{x}')\delta\rho(\mathbf{x}') \, d\mathbf{x}'$$
$$+ \int \mathbf{u}^{(ij)}(\mathbf{x}, \mathbf{x}')\varepsilon_{kl}(\mathbf{x}')\delta\psi_{ijkl}(\mathbf{x}') \, d\mathbf{x}'.$$ (10)

The primary fields $u_i(\mathbf{x}')$ and $\varepsilon_{kl}(\mathbf{x}')$ are found by solving Equation (7) once the force $\mathbf{f}$ is specified. We assume that $\mathbf{f}$ is a point force that follows the same structure as forces described by Equations (5). In this case, one can use reciprocity relations (A.10) or (A.11) from Appendix A to express them in terms of fields generated by sources placed at $\mathbf{x}'$, as illustrated in Figure 1.

In the example later on, we will consider explosive sources at $\mathbf{x}_s$ and volumetric-strain or 'pressure' data φ at $\mathbf{x}_r$. To make Equation (10) applicable to this case, we apply the operator $\nabla_{\mathbf{x}}\cdot$ to $\delta\mathbf{u}(\mathbf{x})$, set $u_i(\mathbf{x}') = u_i^{(0)}(\mathbf{x}', \mathbf{x}_s)$, $\varepsilon_{kl}(\mathbf{x}') = \varepsilon_{kl}^{(0)}(\mathbf{x}', \mathbf{x}_s)$ and use reciprocity relations (A.11). As a result, we get

$$\delta\varphi(\mathbf{x}, \mathbf{x}_s) = -\omega^2 \int \varphi^{(i)}(\mathbf{x}, \mathbf{x}')\varphi^{(i)}(\mathbf{x}_s, \mathbf{x}') \, \delta\rho(\mathbf{x}') \, d\mathbf{x}'$$
$$+ \int \varphi^{(ij)}(\mathbf{x}, \mathbf{x}')\varphi^{(kl)}(\mathbf{x}_s, \mathbf{x}') \, \delta\psi_{ijkl}(\mathbf{x}') \, d\mathbf{x}'.$$ (11)

All the terms on the right-hand side of Equation (11) are obtained from forward simulations with force and momentum sources placed at points $\mathbf{x}'$. For a single scattering point in d space dimensions, this requires $d + \frac{1}{2}d(d+1) = d(d+3)/2$ simulations, 5 in two dimensions and 9 in three dimensions, followed by zero-lag data correlations. If the simulations for the wavefields are carried out with a wavelet, a deconvolution is required in the correlation step. The computational cost can be substantially lower than that of separately simulating all shots of a seismic survey. In the isotropic case, $\delta\psi_{ijkl} = \delta\lambda \; \delta_{ij}\delta_{kl} + \delta\mu \; \left(\delta_{ik}\delta_{jl} + \delta_{il}\delta_{kj}\right)$, where $\delta\lambda$

and $\delta\mu$ are perturbed Lamé parameters. The sum in the second integral in Equation (11) in this case reduces to $\delta\lambda \, \varphi^{(0)}(\mathbf{x}, \mathbf{x}')\varphi^{(0)}(\mathbf{x}_s, \mathbf{x}') + 2\delta\mu \, \varphi^{(ij)}(\mathbf{x}, \mathbf{x}')\varphi^{(ij)}(\mathbf{x}_s, \mathbf{x}')$.

In the next section, we will present a 2-D marine example for the isotropic elastic case. Appendix B summarizes the algorithmic steps for this special case.

NUMERICAL EXAMPLE

To validate the method, we consider an earlier two-dimensional isotropic elastic marine subsurface model (Mulder & Kuvshinov, 2023). The material properties were defined by an index map, repeated here as Figure 2. The negative values refer to four reservoirs, zero is used for seawater and positive values for various layers with piecewise constant elastic properties. Three Born scattering datasets were generated with a finite-difference code for a unit perturbation of ν_k ($k = 1, 2, 3$) at the scatter point $x = 3280$ m, $z = 2460$ m, close to the centroid of the reservoir with index -1. From five shots at the scatter point, 3×199 shots were synthesized with x_s from -2.9 to 7.0 km at a 50-m spacing at depth $z_s = 10$ m and with receiver offsets from $x_r - x_s = 100$ to 6000 m with a 25-m spacing at a depth $z_r = 8$ m. A direct Born computation would require 3×199 shots at twice the cost or $(1+3)\times199$ shots with a series approach.

Figures 3–5 display a comparison of Born data for one shot at $x_s = 0$ and $z_s = 10$ m computed directly with the two coupled systems, in panels (a), the difference between the Born data synthesized for five different source types at the scatter point and the directly computed data (b), and the shortest-offset trace for each approach, with the directly computed and synthesized Born data. There is a good agreement, bearing in mind that reciprocity for the finite-difference solutions only approximately holds. For this test, a grid spacing of 2 m was chosen for a 15-Hz Ricker wavelet, much finer than commonly used.

Figure 6 shows the normalized covariance matrix in terms of $\delta\log I_p$, $\delta\log v_p$ and $\delta\log(v_s/v_p)$, where $I_p = \rho v_p$, at the selected scatterer obtained from the Hessian based on synthesized Born data for all 199 shots. The finite-difference computations were carried out on a grid with a 10-m spacing in this case. In this example, the Hessian was scaled by the model according to $\delta\mathbf{m}^{\top}\mathbf{H}\,\delta\mathbf{m} = (\delta\log\mathbf{m})^{\top}\overline{\mathbf{H}}(\delta\log\mathbf{m})$, leading to $\overline{\mathbf{H}} = \text{diag}(\mathbf{m}_0)\mathbf{H}\,\text{diag}(\mathbf{m}_0)$, where $\text{diag}(\mathbf{m}_0)$ is a diagonal matrix with the components of the vector $\mathbf{m}_0$ on its diagonal.

To obtain the local covariance matrix in an absolute sense, without normalization, the data energy $\frac{1}{2}\|\mathbf{d}_{\text{obs}}\|^2$ is required, together with an estimate of the relative noise level in the data to define ε in Equation (1). In our synthetic example, that would require the forward simulation of the full seismic dataset, at a much higher cost than synthesizing the Born data
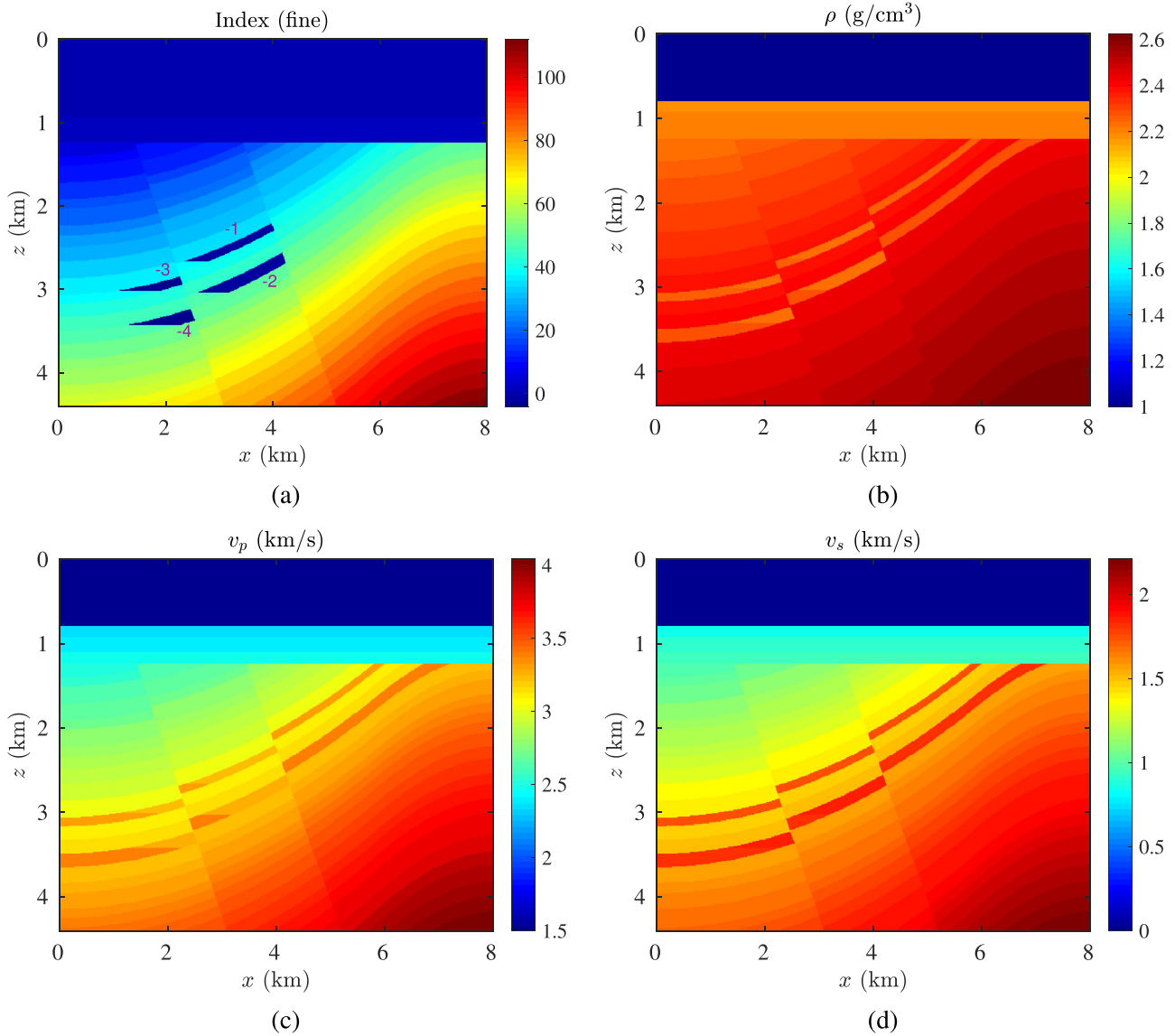
FIGURE 2 An index map (a) defines the piecewise constant values per layer for an isotropic elastic model with (b) density, (c) P- and (d) S-wave velocity. The negative indices correspond to four reservoirs.
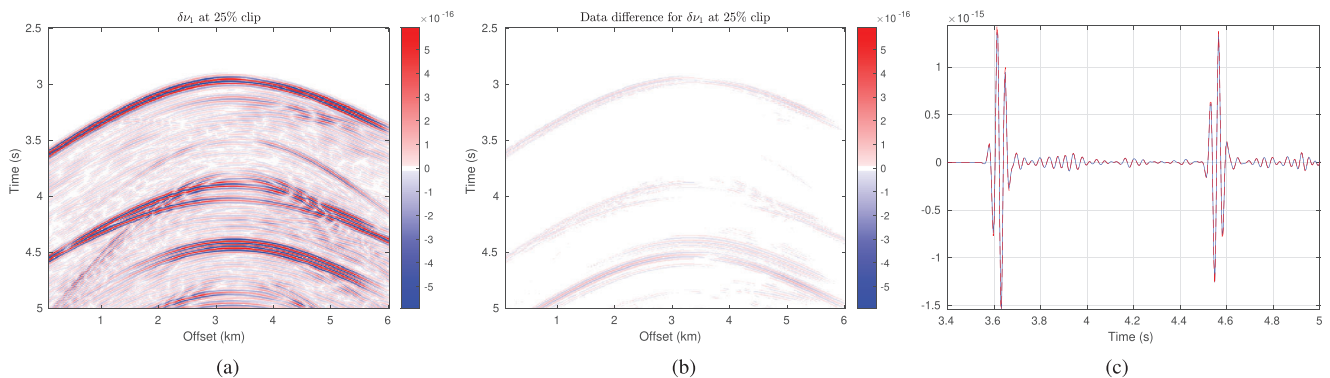

FIGURE 3 (a) Born data for a unit perturbation in one point of $\nu_1 = \rho$ clipped at 25 amplitude. (b) Difference between synthesized Born data and those of (a) at the same scale. (c) Comparison of the shortest-offset trace with Born scattering data (blue) and synthesized Born data based on reciprocity (red, dashed).
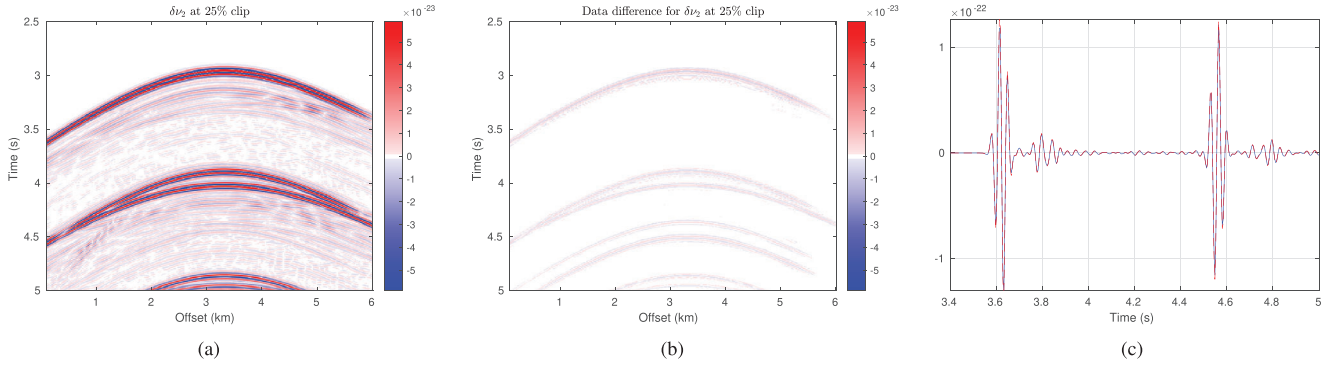
FIGURE 4   As Figure 3, but for a unit perturbation in one point of $\nu_2 = \rho \upsilon_p^2$.
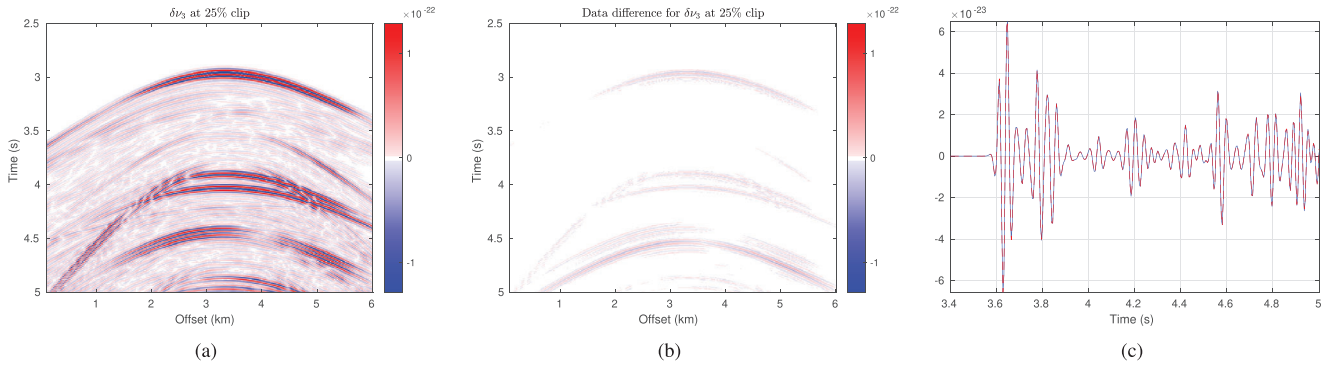

FIGURE 5   As Figure 3, but for $\nu_3 = \rho \upsilon_s^2$.
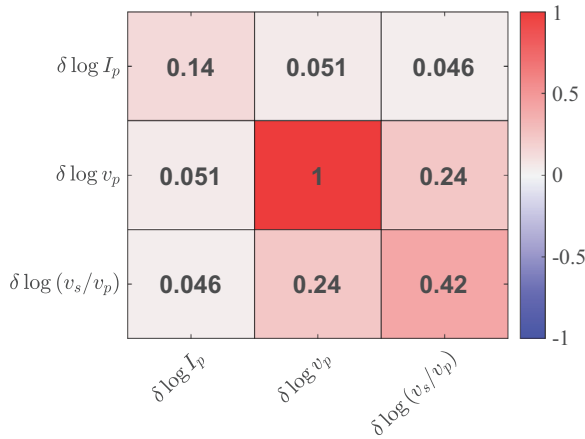

FIGURE 6   Scaled covariance matrix.

via reciprocity. But if the reference model $\mathbf{m}_0$ is the result of full-waveform inversion, this information should already be available.

Specifically, we can consider a weighted norm $\|\mathbf{d}\|^2_{\mathbf{I},\mathbf{W}} = \frac{1}{2}\mathbf{d}^\top\mathbf{W}^\top\mathbf{C}^{-1}_{\text{data}}\mathbf{W}\mathbf{d}$, where $\mathbf{W}$ involves weighting in, for instance, time, frequency and offset and where $\mathbf{C}_{\text{data}}$ is the covariance matrix of the noise. The weighting matrix $\mathbf{W}$ is often used to steer the convergence away from local minima

and accelerate convergence while acting as a preconditioner. It may change during subsequent sets of iterations. In the simplest case of $\mathbf{W} = \mathbf{I}$ and $\mathbf{C}_{\text{data}} = \sigma^2_{\text{data}}\mathbf{I}$ with constant standard deviation σ_{data}, we have $\|\mathbf{d} - \mathbf{d}_{\text{obs}}\|^2_{\mathbf{I},\mathbf{W}} = 2\mathcal{X}/\sigma^2_{\text{data}}$ and condition (1) becomes $\frac{1}{2}(\delta\log\mathbf{m})^\top\overline{\mathbf{H}}(\delta\log\mathbf{m}) \leq \sigma^2_{\text{data}}$ for $\mathbf{g} = \mathbf{0}$ and $\mathcal{X}_0 = 0$.

In this synthetic example, instead of choosing σ^2_{data}, we have scaled the result by the conditional covariance of the $\delta\log\upsilon_p$ perturbation at the scatter point mentioned above, assuming all other parameters are given. Its square root describes the uncertainty in this parameter, typically in the order of 1–10%. Figure 7 displays conditional standard deviations σ_k ($k = 1, 2, 3$), for the parameters $\delta\log I_p$, $\delta\log\upsilon_p$ and $\delta\log(\upsilon_s/\upsilon_p)$, respectively, in all the points of the reservoir with index −1. There is some variation across the region, with, unsurprisingly, the shallower parts being more accurate. In the conditional case, all parameters are assumed to be given, except the one under consideration. The standard deviations are determined by the reciprocal square root of the main diagonal of the Hessian.

At the other extreme, the marginal distribution describes the probability if all parameters are unknown. With our localized approach, such estimates are out of reach and the approach of Mulder and Kuvshinov (2023) may be more
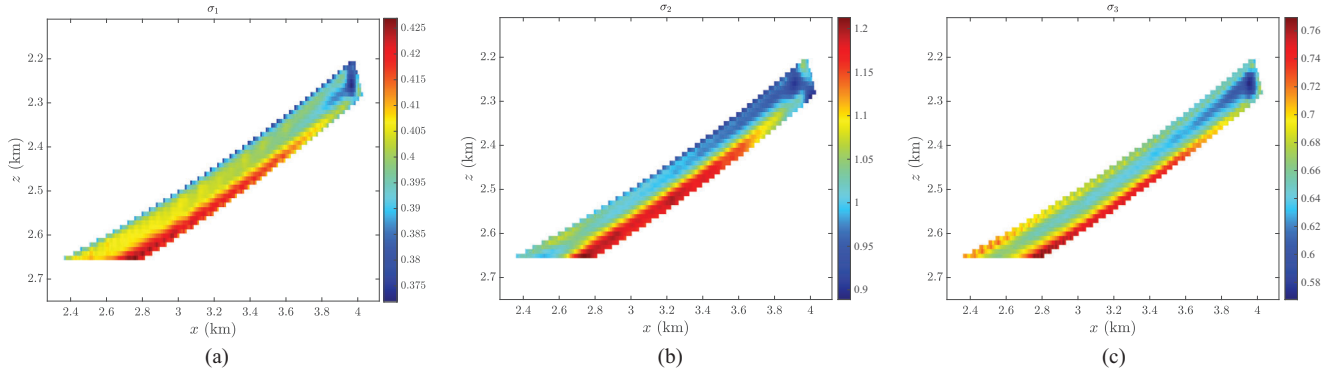
FIGURE 7 Standard deviations for the conditional distribution, scaled to that of the P-wave velocity at one point, for the model parameters (a) $\delta \log I_p$, (b) $\delta \log v_p$ and (c) $\delta \log(v_s/v_p)$ in the reservoir with index -1.
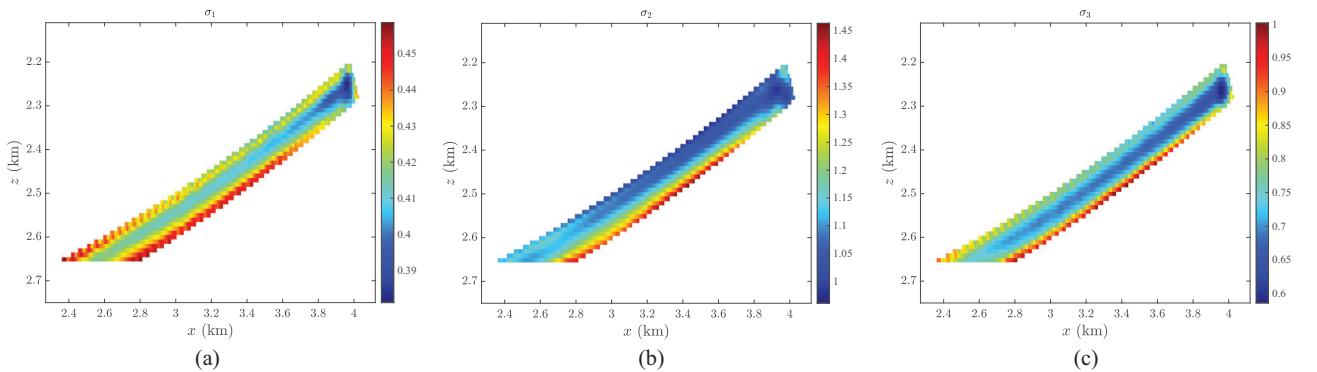

FIGURE 8 As Figure 7, but assuming the three parameters in one point are unknown but given elsewhere.

suitable. Instead, Figure 8 displays the square roots of the diagonal of the block-diagonal covariance matrix, obtained by inverting the block diagonal of the Hessian, consisting of 3×3 blocks. This assumes that all parameters in other points are known, but not those in the point under consideration. Compared to the conditional case, this should increase the estimated standard deviations. The values at the reference scatter point correspond to the square roots of the diagonal of the matrix in Figure 6.

COST ESTIMATES

Table 1 compares the computational cost of four different approaches to compute the wavefields for Born scattering. The number of grid points in d space dimensions is $O(n^d)$. The cost of a single simulation with a finite-difference code is $O(n^{d+1})$ and is taken out as a common factor. The relative cost of modelling is set to 1 and migration costs at least double that amount, adding up to at least 3. The number of shots is n_{shot}, and the number of scatter points is n_{nscat}. For n_{comp} model components, three in the isotropic case, this leads to $n_{comp}n_{nscat}$ model perturbations.

TABLE 1 Relative cost of some methods.

Method	Relative cost
Born data, direct computation	$2n_{shot}n_{comp}n^d$
	or $n_{shot}(1 + n_{comp}n^d)$
Modelling and migration for a sparse subset	$3n_{shot}n_{comp}n_{nscat}$
Born data for geological units or a sparse set	$2n_{shot}n_{comp}n_{nscat}$
	or $n_{shot}(1 + n_{comp}n_{nscat})$
Born data via reciprocity for a small subset	$n_{nscat}d(d+3)/2$

A direct computation of the incoming and scattered field for a unit perturbation of one model component at one grid point yields the cost estimates for the first case in Table 1. The factor 2 accounts for the coupled systems (7) and (8). As already mentioned, the cost can be lowered to $n_{shot}(1 + n_{comp}n^d)$ by using a Taylor-series approach, in which case the incoming field is computed once for all perturbations. The resulting data, however, tend to be noisier. The second case describes modelling followed by migration for a sparse set of model perturbations that are treated all at once, but separately for each model component. The factor 3 accounts for the cost relative to just modelling. If the modelling data are computed for the perturbed model and the migration is carried out in

the reference model, the Born data are fed at data errors into the reverse-time part of the migration and are not explicitly needed for the Hessian.

The third case refers to the use of geological units, connected sets of several points that have the same relative perturbation, each counted as a single scatterer (Mulder & Kuvshinov, 2023). The same estimate is obtained if, instead, a sparse set of n_{nscat} points is considered. The cost is basically the same as for the first case, but with a number of scatterers n_{nscat} much smaller than the number of grid points n^d. The last case refers to the method proposed here and has a cost of the order $n_{\mathrm{nscat}}[d + \frac{1}{2}d(d + 1)]$, equalling $5n_{\mathrm{nscat}}$ in two dimensions and $9n_{\mathrm{nscat}}$ in three dimensions. Note that the number of components does not appear. In this estimate, the cost of synthesizing the data from the numerical wavefields and that of the zero-lag data correlations needed to construct the Hessian have been neglected. Since only scattering data are involved and the interaction with model parameters elsewhere is ignored, only relative uncertainties can be estimated, unless all grid points are considered with $n_{\mathrm{nscat}} = O(n^d)$. The last method will be the least costly if relative covariance matrices have to be found in isolated points or on a dense but small set of points in a target area.

CONCLUSIONS

The computational cost of uncertainty estimation based on a Hessian obtained from Born scattering data can be significantly reduced in target-oriented applications where the model parameters of only a small number of subsurface points are considered. Instead of simulating Born data for an entire seismic survey, only those subsurface points have to be taken as new source positions and all shot and receiver positions of the survey as new receiver positions. For each new source position, several shots with different source characteristics have to be simulated for each force and moment tensor component.

The approach is applicable to evaluate uncertainties associated with perturbations of subsurface blocks whose dimensions do not exceed a fraction of the characteristic wavelength. We have described this approach for a viscoelastic medium and tested it for the simpler 2-D isotropic elastic case. As an illustration, the method was used to determine local estimates of the covariance matrix, which quantifies the relative uncertainties of the elastic model parameters. A cost comparison to alternative methods shows which one is best suited to different circumstances.

DATA AVAILABILITY STATEMENT
Data sharing is not applicable to this article as no new data were created or analysed in this study. However, if the computational results shown in the figures are considered as new data, then the authors elect not to share those.

REFERENCES

Aki, K. & Richards, P.G. (2002) *Quantitative seismology*, 2nd edition. Mill Valley, CA: University Science Books.

Arntsen, B. & Carcione, J.M. (2000) A new insight into the reciprocity principle. *Geophysics*, 65(5), 1604–1612. https://doi.org/10.1190/1.1444848

Backus, G. & Gilbert, F. (1970) Uniqueness in the inversion of inaccurate gross Earth data. *Philosophical Transactions of the Royal Society of London. Series A, Mathematical and Physical Sciences*, 266(1173), 123–192. https://doi.org/10.1098/rsta.1970.0005

Ben-Israel, A. & Greville, T.N.E. (2003) *Generalized inverses, theory and applications*, 2nd edition. New York: Springer. https://doi.org/10.1007/b97366

Betancourt, M. (2018) A conceptual introduction to Hamiltonian Monte Carlo. arXiv. https://doi.org/10.48550/arXiv.1701.02434

Beylkin, G. & Burridge, R. (1990) Linearized inverse scattering problems in acoustics and elasticity. *Wave Motion*, 12(1), 15–52. https://doi.org/10.1016/0165-2125(90)90017-X

Biswas, R., Walker, M., Zhang, J., Paramo, P., Wolf, K., Gerth, S., Winterbourne, J., Roy, A., Morris, P., Decalf, C., Zheng, Y. & Warnick, R. (2023) Bayesian AVA elastic seismic inversion using Stein variational gradient descent (SVGD). In *Proceedings of the 84th EAGE Annual Conference & Exhibition*, volume 2023. Houten, the Netherlands: European Association of Geoscientists & Engineers, pp. 1–5. https://doi.org/10.3997/2214-4609.202310835

Bojarski, N.N. (1983) Generalized reaction principles and reciprocity theorems for the wave equations, and the relationship between the time-advanced and time-retarded fields. *Journal of the Acoustical Society of America*, 71, 281–285. https://doi.org/10.1121/1.389721

Chen, B. & Xie, X.-B. (2015) An efficient method for broadband seismic illumination and resolution analyses. In *SEG Technical program expanded abstracts 2015*. Houston, TX: Society of Exploration Geophysicists, pp. 4227–4231. https://doi.org/10.1190/segam2015-5926976.1

De Hoop, A. (1966) An elastodynamic reciprocity theorem for linear, viscoelastic media. *Applied Scientific Research*, 16, 39–45. https://doi.org/10.1007/BF00384053

De Hoop, A. (1988) Time-domain reciprocity theorems for acoustic wave fields in fluids with relaxation. *Journal of the Acoustical Society of America*, 84, 1877–1882. https://doi.org/10.1121/1.397152

Duane, S., Kennedy, A., Pendleton, B.J. & Roweth, D. (1987) Hybrid Monte Carlo. *Physics Letters B*, 195(2), 216–222. https://doi.org/10.1016/0370-2693(87)91197-X

Ely, G., Malcolm, A. & Poliannikov, O.V. (2018) Assessing uncertainties in velocity models and images with a fast nonlinear uncertainty quantification method. *Geophysics*, 83(2), R63–R75. https://doi.org/10.1190/geo2017-0321.1

Fichtner, A. & van Leeuwen, T. (2015) Resolution analysis by random probing. *Journal of Geophysical Research: Solid Earth*, 120(8), 5549–5573. https://doi.org/10.1002/2015JB012106

Fichtner, A. & Zunino, A. (2019) Hamiltonian nullspace shuttles. *Geophysical Research Letters*, 46(2), 644–651. https://doi.org/10.1029/2018GL080931

Fokkema, J.T. & van den Berg, P.M. (1993) *Seismic applications of acoustic reciprocity*. Amsterdam: Elsevier. https://doi.org/10.1016/C2009-0-10209-X

Hak, B. & Mulder, W.A. (2010) Migration for velocity and attenuation perturbations. *Geophysical Prospecting*, 58(6), 939–952. https://doi.org/10.1111/j.1365-2478.2010.00866.x

Hoffmann, A., Brossier, R., Métivier, L. & Tarayoun, A. (2024) Local uncertainty quantification for 3-D time-domain full-waveform inversion with ensemble Kalman filters: application to a North Sea OBC data set. *Geophysical Journal International*, 237(3), 1353–1383. https://doi.org/10.1093/gji/ggae114

Hudson, J.A. & Heritage, J.R. (1981) The use of the Born approximation in seismic scattering problems. *Geophysical Journal International*, 66(1), 221–240. https://doi.org/10.1111/j.1365-246X.1981.tb05954.x

Ikelle, L.T. & Amundsen, L. (2000) Formulation of the linearized forward problems for multicomponent OBS data in a water/solid configuration using the reciprocity theorem. *Geophysical Journal International*, 141(2), 527–534. https://doi.org/10.1046/j.1365-246x.2000.00111.x

Inoue, H., Fukao, Y., Tanabe, K. & Ogata, Y. (1990) Whole mantle P-wave travel time tomography. *Physics of the Earth and Planetary Interiors*, 59(4), 294–328. https://doi.org/10.1016/0031-9201(90)90236-Q

Izzatullah, M., Alkhalifah, T., Romero, J., Corrales, M., Luiken, N. & Ravasi, M. (2023) Plug-and-play Stein variational gradient descent for Bayesian post-stack seismic inversion. In *Proceedings of the 84th EAGE Annual Conference & Exhibition*, volume 2023. Houten, the Netherlands: European Association of Geoscientists & Engineers, pp. 1–5. https://doi.org/10.3997/2214-4609.202310177

Kazei, V. & Alkhalifah, T. (2019) Scattering radiation pattern atlas: What anisotropic elastic properties can body waves resolve? *Journal of Geophysical Research: Solid Earth*, 124(3), 2781–2811. https://doi.org/10.1029/2018JB016687

Knopoff, L. & Gangi, A.F. (1959) Seismic reciprocity. *Geophysics*, 24(4), 681–691. https://doi.org/10.1190/1.1438647

Lévêque, J.-J., Rivera, L. & Wittlinger, G. (1993) On the use of the checker-board test to assess the resolution of tomographic inversions. *Geophysical Journal International*, 115(1), 313–318. https://doi.org/10.1111/j.1365-246X.1993.tb05605.x

Liu, Q. & Wang, D. (2016) Stein variational gradient descent: a general purpose Bayesian inference algorithm. In Lee, D., Sugiyama, M., Luxburg, U., Guyon, I. & Garnett, R. (Eds.), *Advances in neural information processing systems*, volume 29. Red Hook, NY: Curran Associates, pp. 2378–2386.

Martin, J., Wilcox, L.C., Burstedde, C. & Ghattas, O. (2012) A stochastic Newton MCMC method for large-scale statistical inverse problems with application to seismic inversion. *SIAM Journal on Scientific Computing*, 34(3), A1460–A1487. https://doi.org/10.1137/110845598

Minkoff, S.E. (1996) A computationally feasible approximate resolution matrix for seismic inverse problems. *Geophysical Journal International*, 126(2), 345–359. https://doi.org/10.1111/j.1365-246X.1996.tb05295.x

Mulder, W.A. & Kuvshinov, B.N. (2023) Estimating large-scale uncertainty in the context of full-waveform inversion. In *Proceedings of the 84th EAGE Annual Conference & Exhibition*. Houten, the Netherlands: European Association of Geoscientists & Engineers, pp. 1–5. https://doi.org/10.3997/2214-4609.202310304

Mulder, W.A. & Kuvshinov, B.N. (2024) Accelerating target-oriented elastic full-waveform uncertainty estimation by reciprocity. In *Proceedings of the 85th EAGE Annual Conference & Exhibition (including the Workshop Programme)*, volume 2024. Houten, the Netherlands: European Association of Geoscientists & Engineers, pp. 1–5. https://doi.org/10.3997/2214-4609.202410339

Plessix, R. & Mulder, W.A. (2004) Frequency-domain finite-difference amplitude-preserving migration. *Geophysical Journal International*, 157(3), 975–987. https://doi.org/10.1111/j.1365-246X.2004.02282.x

Pratt, R.G., Shin, C. & Hicks, G.J. (1998) Gauss-Newton and full Newton methods in frequency-space seismic waveform inversion. *Geophysical Journal International*, 133(2), 341–362. https://doi.org/10.1046/j.1365-246X.1998.00498.x

Revelo Obando, B. (2018) Full waveform inversion in a MCMC framework. Master's thesis, Delft University of Technology, Delft, The Netherlands. http://resolver.tudelft.nl/uuid:3232eba7-453d-43a3-a20d-71ee4826f986

Rickett, J.E. (2003) Illumination-based normalization for wave-equation depth migration. *Geophysics*, 68(4), 1371–1379. https://doi.org/10.1190/1.1598130

Riffaud, S., Fernández, M.A. & Lombardi, D. (2024) A low-rank solver for parameter estimation and uncertainty quantification in time-dependent systems of partial differential equations. *Journal of Scientific Computing*, 99(2), 34. https://doi.org/10.1007/s10915-024-02488-3

Rizzuti, G., Siahkoohi, A., Witte, P.A. & Herrmann, F.J. (2020) Parameterizing uncertainty by deep invertible networks: an application to reservoir characterization. In *SEG technical program expanded abstracts 2020*. Houston, TX: Society of Exploration Geophysicists, pp. 1541–1545. https://doi.org/10.1190/segam2020-3428150.1

Shaw, R.K. & Sen, M.K. (2004) Born integral, stationary phase and linearized reflection coefficients in weak anisotropic media. *Geophysical Journal International*, 158(1), 225–238. https://doi.org/10.1111/j.1365-246X.2004.02283.x

Siahkoohi, A., Rizzuti, G., Orozco, R. & Herrmann, F.J. (2023) Reliable amortized variational inference with physics-based latent distribution correction. *Geophysics*, 88(3), R297–R322. https://doi.org/10.1190/geo2022-0472.1

Snieder, R. (1986) 3-D linearized scattering of surface waves and a formalism for surface wave holography. *Geophysical Journal International*, 84(3), 581–605. https://doi.org/10.1111/j.1365-246X.1986.tb04372.x

Snieder, R. (2002) Coda wave interferometry and the equilibration of energy in elastic media. *Physical Review E*, 66, 046615. https://doi.org/10.1103/PhysRevE.66.046615

Tarantola, A. (2005) *Inverse problem theory and methods for model parameter estimation*. Philadelphia, PA: SIAM. https://doi.org/10.1137/1.9780898717921

Thurin, J., Brossier, R. & Métivier, L. (2017) An ensemble-transform Kalman filter: full-waveform inversion scheme for uncertainty estimation. In *SEG technical program expanded abstracts 2017*. Houston,

TX: Society of Exploration Geophysicists, pp. 1307–1313. https://doi.org/10.1190/segam2017-17733053.1

Vasco, D.W., Johnson, L.R. & Marques, O. (2003) Resolution, uncertainty, and whole Earth tomography. *Journal of Geophysical Research: Solid Earth*, 108(B1), ESE 9-1–ESE 9-26. https://doi.org/10.1029/2001JB000412

Wang, W., McMechan, G.A. & Ma, J. (2023) Reweighted variational full-waveform inversions. *Geophysics*, 88(4), R499–R512. https://doi.org/10.1190/geo2021-0766.1

Wapenaar, C.P.A. (1996) Reciprocity theorems for two-way and one-way wave vectors: a comparison. *Journal of the Acoustical Society of America*, 100(6), 3508–3518. https://doi.org/10.1121/1.417250

Wapenaar, K. & Fokkema, J. (1993) Reciprocity theorems for diffusion, flow, and waves. *Journal of Applied Mechanics*, 71(1), 145–150. https://doi.org/10.1115/1.1636792

Zhang, X. & Curtis, A. (2020) Variational full-waveform inversion. *Geophysical Journal International*, 222(1), 406–411. https://doi.org/10.1093/gji/ggaa170

Zhao, Z. & Sen, M.K. (2021) A gradient-based Markov chain Monte Carlo method for full-waveform inversion and uncertainty analysis. *Geophysics*, 86(1), R15–R30. https://doi.org/10.1190/geo2019-0585.1

Zhu, H., Li, S., Fomel, S., Stadler, G. & Ghattas, O. (2016) A Bayesian approach to estimate uncertainty for full-waveform inversion using a priori information from depth migration. *Geophysics*, 81(5), R307–R323. https://doi.org/10.1190/geo2015-0641.1

APPENDIX A: RECIPROCITY IN A GENERAL FORM

For completeness, we derive reciprocity relations for an arbitrary and operator $\mathcal{L}$ acting on functions $\mathbf{u}(\mathbf{x}, t)$ that depend on the spatial coordinate $\mathbf{x}$ and temporal coordinate t. Note that we do not specify the form of the operator $\mathcal{L}$ and do not assume that it is self-adjoint. Let $\mathbf{u}(\mathbf{x}, t)$ and $\mathbf{u}'(\mathbf{x}, t)$ satisfy the equations

$$\mathcal{L}\,\mathbf{u} = \mathbf{s}, \qquad \mathcal{L}^{\dagger}\mathbf{u}' = \mathbf{s}'. \tag{A.1}$$

Here, $\mathbf{s}$ and $\mathbf{s}'$ are source terms and $\mathcal{L}^{\dagger}$ is the adjoint operator with the property $\langle \mathbf{u}', \mathcal{L}\mathbf{u} \rangle = \langle \mathcal{L}^{\dagger}\mathbf{u}', \mathbf{u} \rangle$, where the angular brackets denote the inner product in space combined with convolution or correlation in time,

$$\langle \mathbf{u}, \mathbf{v} \rangle = \iint \mathbf{u}(\mathbf{x}, \tau) \cdot \mathbf{v}(\mathbf{x}, t \mp \tau)\, d\mathbf{x}\, d\tau. \tag{A.2}$$

The choice of the minus sign in Equation (A.2) ensures preservation of causality (Aki & Richards, 2002) and leads to reciprocity relations of the convolution type. Equations (A.1) and (A.2) provide Betti's theorem

$$\langle \mathbf{u}, \mathbf{s}' \rangle = \langle \mathbf{u}', \mathbf{s} \rangle. \tag{A.3}$$

We have assumed that, in any finite volume, $\mathbf{u}$ and $\mathbf{v}$ are zero outside a certain time interval and that they decay sufficiently fast in space, so that the surface integrals vanish as $|\mathbf{x}| \to \infty$. Note that this assumption does not hold in, for instance, the homogeneous case without attenuation, when the amplitude decrease due to geometrical spreading is balanced by the increase of the length or area of the boundary integral. Additional intrinsic or scattering attenuation (see, e.g., Snieder 2002) is required to have sufficient decay at infinity.

We consider sources located at a point $\mathbf{x}_s$ with a temporal amplitude or wavelet $w(t)$:

$$\mathbf{s}(\mathbf{x}, t) = w(t)\,\mathbf{f}(\mathbf{x}), \tag{A.4}$$

where $\mathbf{f}(\mathbf{x})$ is a singular function that vanishes for $\mathbf{x} \neq \mathbf{x}_s$. Let $\mathbf{u}(\mathbf{x}, t; \mathbf{x}_s, w_s)$ and $\mathbf{u}'(\mathbf{x}, t; \mathbf{x}'_s, w'_s)$ be solutions of Equation (A.1) for two sources $\mathbf{s}$ and $\mathbf{s}'$ of type (A.4). We introduce the operator X with the property that the spatial dependence $\mathbf{f}'$ of the source $\mathbf{s}'$ is reconstructed by applying X to $\delta(\mathbf{x} - \mathbf{x}_s)$, where $\mathbf{x}_s$ is the position of the source $\mathbf{s}$:

$$\mathbf{f}'(\mathbf{x}) = X\delta(\mathbf{x} - \mathbf{x}_s). \tag{A.5}$$

Using Equation (A.5), we can cast Equation (A.3) in the form

$$X^{\dagger}\mathbf{u}(\mathbf{x}, t; \mathbf{x}_s, w)\Big|_{\mathbf{x}=\mathbf{x}_s} \star w'(t) = \langle \mathbf{u}', \mathbf{s} \rangle, \tag{A.6}$$

where $X^{\dagger}$ is the adjoint operator, $\int f(\mathbf{x})[X'g(\mathbf{x})]d\mathbf{x} = \int [X^{\dagger}f(\mathbf{x})]g(\mathbf{x})d\mathbf{x}$, and the star $\star$ denotes temporal convolution or correlation, depending on the choice of sign in Equation (A.2): $f(t) \star g(t) = \int f(\tau)g(t \mp \tau)\, d\tau$.

We consider point forces $\mathbf{f}$ of the form (5) and denote the correspondent sources by $\mathbf{s}^{(\alpha)}$, $\mathbf{s}^{(\alpha\beta)}$ and $\mathbf{s}^{(0)}$. The solutions of Equation (A.1) are labelled as in $\mathbf{u}^{(\alpha)}$, $\mathbf{u}^{(\alpha\beta)}$ and $\mathbf{u}^{(\alpha\beta\gamma)}$. We use the same labelling as above, although the solutions considered here are different in that respect that they are generated by time-dependent sources and are given in the time domain.

Equation (A.6) implies

$$X^{\dagger}\mathbf{u}^{(\alpha)}(\mathbf{x}, t; \mathbf{x}_s, w)\Big|_{\mathbf{x}=\mathbf{x}_s} \star w'(t) = u'_{\alpha}(\mathbf{x}_s, t; \mathbf{x}'_s, w') \star w(t), \tag{A.7a}$$

$$X^{\dagger}\mathbf{u}^{(\alpha\beta)}(\mathbf{x}, t; \mathbf{x}_s, w)\Big|_{\mathbf{x}=\mathbf{x}_s} \star w'(t) = -\varepsilon'_{\alpha\beta}(\mathbf{x}_s, t; \mathbf{x}'_s, w') \star w(t), \tag{A.7b}$$

where $\varepsilon'_{\alpha\beta} = \frac{1}{2}(\partial_{x_\beta} u'_\alpha + \partial_{x_\alpha} u'_\beta)$. The operators $X^{(i)}$ and $X^{(ij)}$ with the properties

$$X^{(i)} f(\mathbf{x}) = f(\mathbf{x} + \Delta\mathbf{x})\mathbf{e}_i,$$

$$X^{(ij)} f(\mathbf{x}) = \frac{1}{2}\left(\mathbf{e}_i \partial_{x_j} + \mathbf{e}_j \partial_{x_i}\right) f(\mathbf{x} + \Delta\mathbf{x}), \qquad \text{(A.8)}$$

where $\mathbf{e}_i$ is the ith coordinate vector and $\Delta\mathbf{x} = \mathbf{x}_s - \mathbf{x}'_s$, satisfy Equation (A.5) with $\mathbf{s} = \mathbf{s}'^{(i)}$ and $\mathbf{s} = \mathbf{s}'^{(ij)}$ respectively. The actions of adjoint operators on $\mathbf{u}(\mathbf{x}, t)$ are determined by the relations

$$X^{(i)\dagger} \mathbf{u}(\mathbf{x}, t) = u_i(\mathbf{x} - \Delta\mathbf{x}, t),$$

$$X^{(ij)\dagger} \mathbf{u}(\mathbf{x}, t) = -\varepsilon_{ij}(\mathbf{x} - \Delta\mathbf{x}, t), \qquad \text{(A.9)}$$

where $\varepsilon_{\alpha\beta} = \frac{1}{2}(\partial_{x_\beta} u_\alpha + \partial_{x_\alpha} u_\beta)$. Considering Equations (A.7a) and (A.7b) for the cases where the field $\mathbf{u}'$ is created by the sources $\mathbf{s}' = \mathbf{s}'^{(i)}$, and $\mathbf{s}' = \mathbf{s}'^{(ij)}$, and using Equation (A.9), we obtain

$$u_i^{(\alpha)}(\mathbf{x}'_s, t; \mathbf{x}_s, w) \star w'(t) = u_\alpha'^{(i)}(\mathbf{x}_s, t; \mathbf{x}'_s, w') \star w(t),$$
$$\text{(A.10a)}$$

$$u_i^{(\alpha\beta)}(\mathbf{x}'_s, t; \mathbf{x}_s, w) \star w'(t) = -\varepsilon_{\alpha\beta}'^{(i)}(\mathbf{x}_s, t; \mathbf{x}'_s, w') \star w(t),$$
$$\text{(A.10b)}$$

$$\varepsilon_{ij}^{(\alpha)}(\mathbf{x}'_s, t; \mathbf{x}_s, w) \star w'(t) = -u_\alpha'^{(ij)}(\mathbf{x}_s, t; \mathbf{x}'_s, w') \star w(t),$$
$$\text{(A.10c)}$$

$$\varepsilon_{ij}^{(\alpha\beta)}(\mathbf{x}'_s, t; \mathbf{x}_s, w) \star w'(t) = \varepsilon_{\alpha\beta}'^{(ij)}(\mathbf{x}_s, t; \mathbf{x}'_s, w') \star w(t).$$
$$\text{(A.10d)}$$

The reciprocity relations for the source that creates a force proportional to the gradient of the delta-function, $s_i^{(0)} = w(t) \partial_{x_i} \delta(\mathbf{x} - \mathbf{x}_s)$, follow from Equations (A.10) by noticing that $s_i^{(0)} = \sum_{\alpha,\beta} \mathbf{s}^{(\alpha\beta)}$:

$$u_i^{(0)}(\mathbf{x}'_s, t; \mathbf{x}_s, w) \star w'(t) = -\varphi'^{(i)}(\mathbf{x}_s, t; \mathbf{x}'_s, w') \star w(t),$$
$$\text{(A.11a)}$$

$$\varepsilon_{ij}^{(0)}(\mathbf{x}'_s, t; \mathbf{x}_s, w) \star w'(t) = \varphi'^{(ij)}(\mathbf{x}_s, t; \mathbf{x}'_s, w') \star w(t),$$
$$\text{(A.11b)}$$

where $\varphi' = \sum_\alpha \varepsilon'_{\alpha\alpha}$. Reciprocity relation (A.10b) can also be obtained by substituting Equation (A.10a) into Equation (6). Equation (A.10c) is the same as (A.10b), where the variables with primes and without primes are swapped. Equation (A.10d) follows from Equation (6) with the replacement $\mathbf{u}^{(\alpha)} \rightarrow \varepsilon_{ij}^{(\alpha)}$ and Equation (A.10c).

APPENDIX B: THE 2-D MARINE ISOTROPIC CASE

The algorithmic steps for the special case of an isotropic elastic model in 2D with a pressure source and recorded pressure data are summarized.

The source types are

$$\mathbf{F}_x = \begin{pmatrix} 1 \\ 0 \end{pmatrix}, \quad \mathbf{F}_z = \begin{pmatrix} 0 \\ 1 \end{pmatrix}, \qquad \text{(B.1a)}$$

$$\mathbf{M}_{xx} = \begin{pmatrix} 1 & 0 \\ 0 & 0 \end{pmatrix}, \quad \mathbf{M}_{zz} = \begin{pmatrix} 0 & 0 \\ 0 & 1 \end{pmatrix}, \quad \mathbf{M}_{xz} = \begin{pmatrix} 0 & 1 \\ 1 & 0 \end{pmatrix}. \qquad \text{(B.1b)}$$

The pressure $p = -\rho v_p^2 \varphi$, with $\varphi = \nabla \cdot \mathbf{u}$ for displacements $\mathbf{u}$. The data for the various sources are denoted by $\varphi^{(1)}$ for $\mathbf{F}_x$, $\varphi^{(2)}$ for $\mathbf{F}_z$, $\varphi^{(3)}$ for $\mathbf{M}_{xx}$, $\varphi^{(4)}$ for $\mathbf{M}_{zz}$ and $\varphi^{(5)}$ for $\mathbf{M}_{xz}$. The sources are located at $\mathbf{x}_p$ and the data $\varphi^{(k)}$ are recorded at $\mathbf{x}_s$ and $\mathbf{x}_r$. To simplify the notation, we use the abbreviations $\varphi_r^{(k)} = \varphi^{(k)}(\mathbf{x}_r; \mathbf{x}_p)$ and $\varphi_s^{(k)} = \varphi^{(k)}(\mathbf{x}_s; \mathbf{x}_p)$.

In the frequency domain, let

$$b_{1,s,r} = -\frac{\omega^2}{w}\left(\varphi_r^{(1)} \varphi_s^{(1)} + \varphi_r^{(2)} \varphi_s^{(2)}\right), \qquad \text{(B.2)}$$

for $\delta\rho = \delta(\mathbf{x} - \mathbf{x}_p)$. Here, w is the wavelet, used for the sources at $\mathbf{x}_p$. For $\delta(\rho v_p^2) = \delta(\mathbf{x} - \mathbf{x}_p)$, we define

$$b_{2,s,r} = \frac{1}{w}\left(\varphi_r^{(3)} + \varphi_r^{(4)}\right)\left(\varphi_s^{(3)} + \varphi_s^{(4)}\right), \qquad \text{(B.3)}$$

and for $\delta(\rho v_s^2) = \delta(\mathbf{x} - \mathbf{x}_p)$,

$$b_3 = b_{33} + 2(b_{31} + b_{32} - b_2), \qquad \text{(B.4)}$$

with

$$b_{3k,s,r} = \varphi_r^{(k+2)} \varphi_s^{(k+2)}/w \quad \text{for } k = 1, 2, 3. \qquad \text{(B.5)}$$

The data $b_{k,s,r}$ $(k = 1, 2, 3)$ can then be multiplied by $-\rho v_p^2$ at the receiver enumerated by $r = r(s)$ to obtain the pressure.

The local Hessian $\mathbf{H}$ is formed by correlating the data: $H_{ij} = \sum_s \sum_{r(s)} \text{Re}\left(b_{i,s,r(s)} b_{j,s,r(s)}^*\right)$, summed over all receivers and shots, enumerated by $r(s)$ and s, respectively. The asterisk denotes the complex conjugate. The transformation from the model parameters ρ, ρv_p^2 and ρv_s^2 to $\delta \log(I_p)$, $\delta \log(v_p)$, $\delta \log(v_p/v_s)$ requires the evaluation of $\bar{\mathbf{H}} = \mathbf{B}_1^T \mathbf{B}_0^T \mathbf{H} \mathbf{B}_0 \mathbf{B}_1$, with $\mathbf{B}_0 = \text{diag}(\rho, \rho v_p^2, \rho v_s^2)$ and

$$\mathbf{B}_1 = \begin{pmatrix} 1 & -1 & 0 \\ 1 & 1 & 0 \\ 1 & 1 & 2 \end{pmatrix}. \qquad \text{(B.6)}$$

In three dimensions, the expressions are similar but there are nine source types instead of five and, accordingly, the summations involve more terms.